

Finite difference formulas in the complex plane

Bengt Fornberg *

Department of Applied Mathematics, University of Colorado, Boulder, CO 80309, USA

October 25, 2021

Abstract

Among general functions of two variables $f(x, y)$, analytic functions $f(z)$ with $z = x + iy$ form a very important special case. One consequence of analyticity turns out to be that 2-D finite difference (FD) formulas can be made remarkably accurate already for small stencil sizes. This article discusses some key properties of such complex plane FD formulas. Application areas include numerical differentiation, interpolation, contour integration, and analytic continuation.

Keywords: Finite differences, complex variables, analytic functions, Euler-Maclaurin, contour integration, analytic continuation.

Mathematics Subject Classification: Primary: 30-08, 30-E10, 65D25; Secondary: 30B40, 30E20, 65E99.

1 Introduction

Finite difference (FD) formulas were widely used already in the 19th century, for tasks such as interpolation and numerical solution of ODEs. Their use for approximating PDEs, with stencils most commonly formed by combining 1-D approximations in the separate directions on a Cartesian grid, dates back to around 1910 [20]. Surveys of FD approximations include [12, 17]. Tables 1 and 2 give the weights for some centered FD approximations for the first and second derivative.

While the calculation of FD weights and their subsequent applications (in particular to PDEs) is extensively documented in the literature¹, the same cannot be said of FD approximations in the complex plane, applied to analytic functions. Reasons why such formulas can feature remarkably high orders of accuracy without extending far from the point of approximation include

1. A derivative $f^{(k)}(z_0)$ depends equally much on data from all directions surrounding z_0 (which, with no loss of generality, can be set to $z_0 = 0$)², i.e., stencils should not extend far out just along a line, and

**Email:* fornberg@colorado.edu , ORCID 0000-0003-0014-6985

¹Chapter 1 of [12] gives several algorithms for computing FD weights in 1-D on either equi-spaced or irregularly spaced nodes, with its later chapters focusing on non-Cartesian node layouts in multiple dimensions.

²cf., equation (3) below.

order	weights										
2					$-\frac{1}{2}$	0	$\frac{1}{2}$				
4				$\frac{1}{12}$	$-\frac{2}{3}$	0	$\frac{2}{3}$	$-\frac{1}{12}$			
6			$-\frac{1}{60}$	$\frac{3}{20}$	$-\frac{3}{4}$	0	$\frac{3}{4}$	$-\frac{3}{20}$	$\frac{1}{60}$		
8		$\frac{1}{280}$	$-\frac{4}{105}$	$\frac{1}{5}$	$-\frac{4}{5}$	0	$\frac{4}{5}$	$-\frac{1}{5}$	$\frac{4}{105}$	$-\frac{1}{280}$	
10	$-\frac{1}{1260}$	$\frac{5}{504}$	$-\frac{5}{84}$	$\frac{5}{21}$	$-\frac{5}{6}$	0	$\frac{5}{6}$	$-\frac{5}{21}$	$\frac{5}{84}$	$-\frac{5}{504}$	$\frac{1}{1260}$
\vdots	\cdots	\downarrow	\downarrow	\downarrow	\downarrow	\vdots	\downarrow	\downarrow	\downarrow	\downarrow	\cdots
limit	\cdots	$\frac{1}{4}$	$-\frac{1}{3}$	$\frac{1}{2}$	-1	0	1	$-\frac{1}{2}$	$\frac{1}{3}$	$-\frac{1}{4}$	\cdots

Table 1: Weights for centered FD approximations of the first derivative on a grid with spacing h (omitting the factor $1/h$).

order	weights										
2					1	-2	1				
4				$-\frac{1}{12}$	$\frac{4}{3}$	$-\frac{5}{2}$	$\frac{4}{3}$	$-\frac{1}{12}$			
6			$\frac{1}{90}$	$-\frac{3}{20}$	$\frac{3}{2}$	$-\frac{49}{18}$	$\frac{3}{2}$	$-\frac{3}{20}$	$\frac{1}{90}$		
8		$-\frac{1}{560}$	$\frac{8}{315}$	$-\frac{1}{5}$	$\frac{8}{5}$	$-\frac{205}{72}$	$\frac{8}{5}$	$-\frac{1}{5}$	$\frac{8}{315}$	$-\frac{1}{560}$	
10	$\frac{1}{3150}$	$-\frac{5}{1008}$	$\frac{5}{126}$	$-\frac{5}{21}$	$\frac{5}{3}$	$-\frac{5269}{1800}$	$\frac{5}{3}$	$-\frac{5}{21}$	$\frac{5}{126}$	$-\frac{5}{1008}$	$\frac{1}{3150}$
\vdots	\cdots	\downarrow	\downarrow	\downarrow	\downarrow	\downarrow	\downarrow	\downarrow	\downarrow	\downarrow	\cdots
limit	\cdots	$-\frac{2}{4^2}$	$\frac{2}{3^2}$	$-\frac{2}{2^2}$	$\frac{2}{1^2}$	$-\frac{\pi^2}{3}$	$\frac{2}{1^2}$	$-\frac{2}{2^2}$	$\frac{2}{3^2}$	$-\frac{2}{4^2}$	\cdots

Table 2: Weights for centered FD approximations of the second derivative (omitting the factor $1/h^2$).

2. The Cauchy-Riemann equations (defined below in (2)) put constraints on the range of functions that need to be considered.

General background about complex variables and analytic functions (however, without any discussion of computational aspects) can be found for example in [3, 13]. The focus of this current study is to present the main features of FD counterparts in the complex plane, applied to functions that are known to be analytic.

2 Finite difference formulas in the complex plane

Analytic functions form a very important special case of functions defined over a 2-D x, y -plane. A function $f(z)$ with $z = x + iy$ is said to be analytic if $\frac{df}{dz} = \lim_{\Delta z \rightarrow 0} \frac{f(z+\Delta z) - f(z)}{\Delta z}$ is uniquely defined, no matter from which direction in the complex plane Δz approaches zero. One immediate consequence is that one need not distinguish $\frac{\partial f}{\partial x}$ from $\frac{\partial f}{\partial y}$. This in turn implies that, separating $f(z)$ into real and imaginary parts

$$f(z) = u(x, y) + i v(x, y), \tag{1}$$

these parts will satisfy the Cauchy-Riemann (CR) equations³

$$\frac{\partial u}{\partial x} = \frac{\partial v}{\partial y}, \quad \frac{\partial u}{\partial y} = -\frac{\partial v}{\partial x}. \tag{2}$$

Any function $f(x)$ that possesses a Taylor expansion at some x -location can be extended to an analytic function, with a vast range of further consequences.⁴

Let L be a linear operator that we wish to approximate at some point (which, without loss of generality, we set to $z = 0$) by using weights w_k at surrounding nodes z_k , $k = 1, 2, \dots, N$ (which typically will include $z = 0$). Examples of such operators include derivatives $\frac{d^k}{dz^k}$, $k = 1, 2, 3, \dots$. Two straightforward ways to determine the weights w_k (neither requiring more than about 3-4 lines of code) for analytic function FD stencils are:⁵

Method 1: Form and solve the linear system that enforces the exact result when applied to as many of the test functions $1, z, z^2, z^3, \dots$ as possible, and

Method 2: Enforce that the Taylor expansion (in ξ) of $\sum_{k=1}^N w_k e^{z_k \xi}$ matches that of $Le^{z\xi}|_{z=0}$ to as many powers of ξ as possible.

A third method, giving explicit weight expressions, is used for analysis in Section 8. For floating point calculations, the first method is particularly convenient. The second method applies more directly in a wider range of contexts (as noted at the end of Section 3.1). Appendix A gives brief codes for the two methods, in MATLAB and Mathematica, respectively, when applied to the case of finding centered FD weights for the the second derivative on a stencil of size 5×5 (with

³The reverse statement, that the CR equations imply analyticity, requires only slight ‘fine print’, to rule out cases such as $f(z) = e^{-1/z^4}$, for which the CR equations hold also at the point of discontinuity $z = 0$.

⁴As surveyed in text books on analytic functions, e.g., [3, 13].

⁵Chapter 1 in [12] provides a summary of FD methods, including Method 1. Method 2 produces the identical linear system to solve (differing only in how the equations are scaled).

comments indicating where the operator and the stencil type are specified, to make generalizations straightforward).

In both methods, the coefficient matrix becomes of Vandermonde type

$$A = \begin{bmatrix} 1 & 1 & \dots & 1 \\ z_1^1 & z_2^1 & & z_N^1 \\ \vdots & & & \vdots \\ z_1^{N-1} & z_2^{N-1} & \dots & z_N^{N-1} \end{bmatrix}.$$

Matrices of this type are non-singular, as long as the nodes z_k are distinct. This can be seen by writing $z_N = z$. Then, $\det(A)$ becomes a polynomial in z of degree $N - 1$, with all its $N - 1$ zeros accounted for by (the not permitted) cases $z = z_1, \dots, z = z_{N-1}$.

2.1 Examples of centered FD stencils

By either of the methods for calculating weights, one obtains for example the following 3×3 stencils (i.e., with $N = 9$; centered at the origin and with grid spacing h):

$$f'(0) = \frac{1}{40h} \begin{bmatrix} -1 - i & -8i & 1 - i \\ -8 & 0 & 8 \\ -1 + i & 8i & 1 + i \end{bmatrix} f + O(h^8),$$

$$f''(0) = \frac{1}{20h^2} \begin{bmatrix} i & -8 & -i \\ 8 & 0 & 8 \\ -i & -8 & i \end{bmatrix} f + O(h^7),$$

$$f^{(3)}(0) = \frac{3}{40h^3} \begin{bmatrix} 1 - i & 16i & -1 - i \\ -16 & 0 & 16 \\ 1 + i & -16i & -1 + i \end{bmatrix} f + O(h^6),$$

$$f^{(4)}(0) = \frac{3}{10h^4} \begin{bmatrix} -1 & 16 & -1 \\ 16 & -60 & 16 \\ -1 & 16 & -1 \end{bmatrix} f + O(h^5),$$

etc., up through the approximation for $f^{(8)}(0)$ that is discussed in different contexts in Sections 4 and 5. Counterpart formulas for 5×5 stencils are given in Appendix B.

2.2 Discussion

Numerical evaluation of high order derivatives based only on function values along the real axis is a severely ill-conditioned task. Cauchy's integral formula

$$f^{(k)}(z_0) = \frac{k!}{2\pi i} \oint_{\Gamma} \frac{f(z)}{(z - z_0)^{k+1}} dz, \quad k = 0, 1, 2, \dots \quad (3)$$

provides a much more stable option, as was noted in [1, 18, 19]. A key issue when using (3) becomes how to best choose the integration path Γ (which must encircle z_0 once in the positive direction, but not include any singularity of $f(z)$). This has been addressed in [5, 6]. The present FD stencils similarly use function values for $f(z)$ in a singularity-free region surrounding z_0 , and require a choice of step size h in place of choosing a path to discretize along. There are different contexts in which analytic functions are numerically available on grids:

- Visualization of analytic functions is increasingly often used, and is virtually always grid-based.
- Some analytic functions are most effectively calculated over gridded domains,⁶
- The present study was partly motivated by an application in mineral prospecting. Magnetic and gravitational field variations can be measured from an airplane flying along successive parallel straight paths over an area of interest, obtaining measurements at equi-spaced locations. Numerical Hilbert transforms followed by complex plane differentiations form key post-processing steps [15].

FD formulas can re-purpose such grid-based data for a variety of different tasks, without needing additional function evaluations at method-specific locations (as required for example when using Gaussian quadrature).

3 Application of FD stencils to Euler-Maclaurin expansions

Asymptotic formulas arise in many applications, and may take the form of powers of some discretization step h together with coefficients involving increasing order derivatives. Examples include two common versions of the Euler-Maclaurin formula, which can be seen as error expansions of the trapezoidal rule (TR) and the midpoint rule, respectively. We summarize next the discussions in [9, 10].

3.1 The Euler-Maclaurin formulas

In the case of a semi-infinite interval $[x_0, \infty]$, with nodes at $x_k = x_0 + kh$ and at $\xi_k = x_0 + (k + \frac{1}{2})h$, $k = 0, 1, 2, \dots$, respectively, these are

$$\int_{x_0}^{\infty} f(x)dx - h \sum_{k=0}^{\infty} f(x_k) \approx -\frac{h}{2}f(x_0) + \frac{h^2}{12}f^{(1)}(x_0) - \frac{h^4}{720}f^{(3)}(x_0) + \frac{h^6}{30240}f^{(5)}(x_0) - \frac{h^8}{1209600}f^{(7)}(x_0) + \dots, \quad (4)$$

and

$$\int_{x_0}^{\infty} f(x)dx - h \sum_{k=0}^{\infty} f(\xi_k) \approx -\frac{h^2}{24}f^{(1)}(x_0) + \frac{7h^4}{5760}f^{(3)}(x_0) - \frac{31h^6}{967680}f^{(5)}(x_0) + \frac{127h^8}{154828800}f^{(7)}(x_0) + \dots \quad (5)$$

In both cases, the coefficients are expressible in terms of Bernoulli numbers; cf., [8], Appendix A. Applications include approximating infinite sums in cases where the function can be analytically integrated. In case of finite intervals, the expansions can be applied separately at the two ends.

⁶such as the Painlevé transcendents, cf., [14].

An alternate usage is then to approximate integrals by means of finite sums, as described below in Section 3.2.

In the case that only equi-spaced function data is available, the derivatives in (4) and (5) can be replaced by regular FD approximations that extend only along the x -direction, described for centered approximation in [8], and for one-sided approximations (that do not extend outside the interval) in [11]. However, if function values are available surrounding x_0 in the complex plane, FD formulas that utilize this provide a very attractive alternative.

Method 1: For both (4) and (5), the right hand sides (RHSs) can straightforwardly be approximated by complex plane FD stencils, with the increasing powers of h perfectly balanced by the powers of h in the denominators of these stencils. One strategy becomes to decide on a stencil size (such as 3×3 , 5×5 , or 7×7) and then approximate as many terms / derivatives as this size permits, followed by adding these up according to their coefficients.

With no loss of generality, we set $x_0 = 0$ and schematically write the regular TR (including only the first term in the RHS of (4)) as

$$\int_0^\infty f(x)dx = h \left\{ \frac{1}{2} \quad 1 \quad 1 \quad 1 \quad 1 \quad 1, \dots \right\} f + O(h^2). \quad (6)$$

For example, with 3×3 stencils, odd order derivatives up through $f^{(7)}(0)$ can be approximated. Added together, we obtain an end correction to the trapezoidal rule (TR) that can similarly be summarized as

$$\int_0^\infty f(x)dx = h \left\{ \left[\begin{array}{ccc} \boxed{\frac{-821-779i}{403200}} & \boxed{\frac{-1889i}{100800}} & \boxed{\frac{821-779i}{403200}} \\ \boxed{\frac{-1511}{100800}} & \left\{ \frac{1}{2} \right\} & \boxed{\frac{1511}{100800}} \\ \boxed{\frac{-821+779i}{403200}} & \boxed{\frac{1889i}{100800}} & \boxed{\frac{821+779i}{403200}} \end{array} \right] \quad 1 \quad 1 \quad 1 \quad 1, \dots \right\} f + O(h^{10}), \quad (7)$$

where the added 'correction terms' have been boxed. This approach is discussed in [9], in the context of integrating an analytic function along finite line segments on an equi-spaced grid. With a 5×5 stencil, the accuracy becomes $O(h^{26})$; in general one more than the number of nodes in the stencil. Figure 1 illustrates that the correction coefficients are numerically very small compared to the regular weights in the TR.

Method 2: This produces identical TR corrections more directly, as it requires no knowledge of the Euler-Maclaurin expansion (4). The LHS of (4), applied to $e^{z\xi}$, becomes (when converging) $\int_0^\infty e^{z\xi} dz - h \sum_{k=0}^\infty e^{kh\xi} = \frac{h}{e^{h\xi}-1} - \frac{1}{\xi}$. This expression is then substituted in place of ξ^2 in the second line of the Mathematica code in Appendix A, producing the same FD stencil (for TR end correction) as obtained by Method 1.

3.2 Application to integration around a closed contour

We consider next one of the test problems discussed more extensively in [9, 10]: Integrate

$$f(z) = \frac{2}{z - 0.4(1+i)} - \frac{1}{z + 0.4(1+i)} + \frac{1}{z + (1.2 - 1.6i)} - \frac{3}{z - (1.3 + 2i)}, \quad (8)$$

around the rectangle indicated by red dots in Figure 2. The green dots indicate the additional function values used when end-correcting each line segment by a 5×5 stencil, as illustrated in

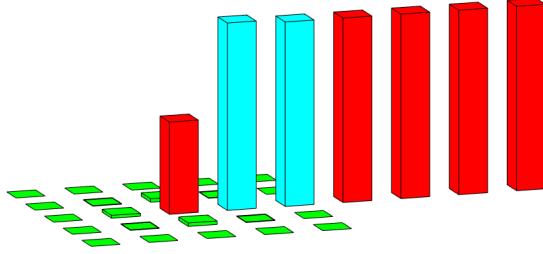


Figure 1: Illustration of the magnitudes of the weights in the 5×5 case of TR end correction. Entries belonging to the TR formula are shown in red, to the correction stencil in green, and the overlapping entries in blue. Compared to the TR weights ($1/2$ at the end point(s), and 1 otherwise), the correction stencil weights are two (or more) orders of magnitude smaller. The exact correction weights in this 5×5 stencil case are given in [9].

Figure 1. Figure 3 shows the rates at which the errors go to zero as h decreases. The errors originating from the path corners in the 5×5 case are so low that, for relatively large h (to the left in the figure), the total error becomes instead dominated by the TR along the interior of the line segments. Also these errors can be further improved on, as described in [10].

4 Test of analyticity

For a general function of two variables $f(x, y)$ (not necessarily analytic), Taylor expansion in x and y will show that

$$\frac{1}{6h^2} \begin{bmatrix} 1 & 4 & 1 \\ 4 & -20 & 4 \\ 1 & 4 & 1 \end{bmatrix} f = \left(\frac{\partial^2}{\partial x^2} + \frac{\partial^2}{\partial y^2} \right) f + O(h^2), \quad (9)$$

matching the highest order of accuracy that is possible for a 3×3 size stencil approximating the Laplacian operator. Nevertheless, in the particular context of solving Laplace's equation $\frac{\partial^2 f}{\partial x^2} + \frac{\partial^2 f}{\partial y^2} = 0$, one finds (again by Taylor expansion⁷) that this same stencil then becomes accurate to $O(h^6)$. If we next consider the case of $f(z)$ either analytic or harmonic, we therefore obtain

$$\begin{bmatrix} 1 & 4 & 1 \\ 4 & -20 & 4 \\ 1 & 4 & 1 \end{bmatrix} f = 0 + O(h^8). \quad (10)$$

In contrast, if the function $f(z)$ is not analytic, applying this stencil to a general function $f(x, y)$ will typically give a much larger result than $O(h^8)$, making the application of this stencil a rough (but still often useful) numerical test of analyticity.

From the perspective of FD formulas for analytic functions, one can note that

$$f^{(8)}(0) = \frac{504}{h^8} \begin{bmatrix} 1 & 4 & 1 \\ 4 & -20 & 4 \\ 1 & 4 & 1 \end{bmatrix} f + O(h^1) \quad (11)$$

⁷See for ex. [12], Section 1.2.2.

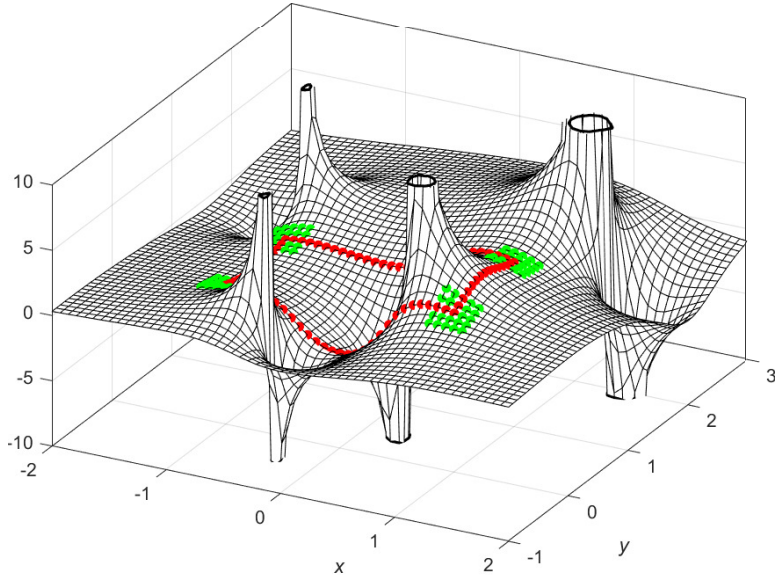


Figure 2: Real part of the test function (8), with the integration contour shown by the red dots.

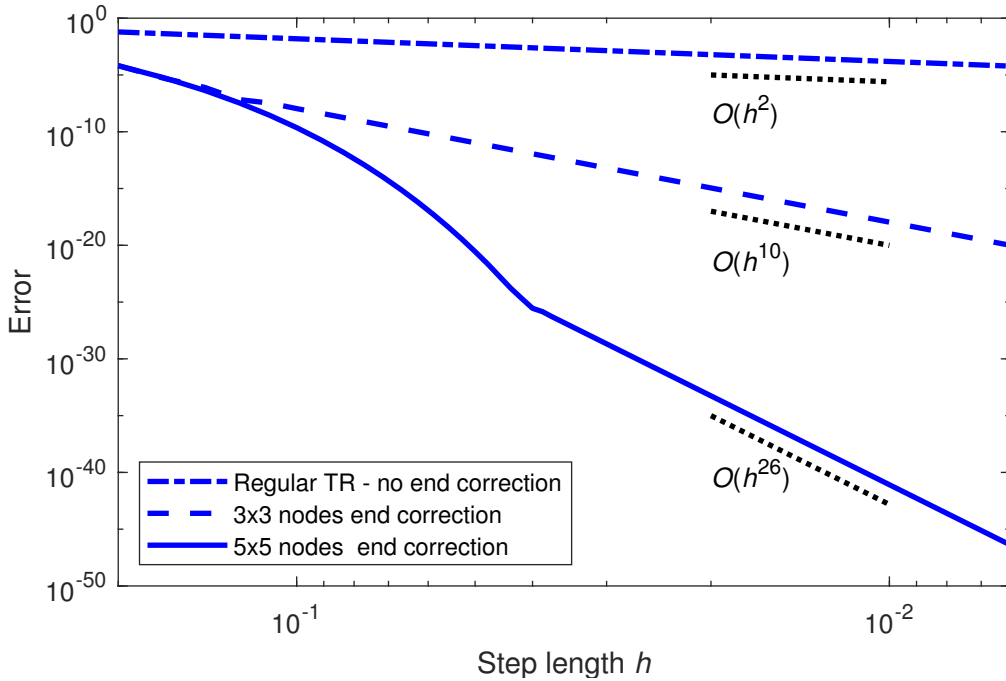


Figure 3: Log-log plot of the error for the test problem described in Section 3.2. With the grid spacing $h \approx 0.07$ shown in Figure 2, the errors for the three approximations are roughly 10^{-2} , 10^{-9} , and 10^{-15} , respectively. Roughly speaking, the grid density needed for a ‘reasonably resolved’ functional display is comparable to what is needed for double precision integration accuracy.

contains a multiple of this same stencil. This observation generalizes to provide a systematic way to obtain nontrivial stencils evaluating to zero particularly closely for analytic functions, i.e., find the FD formula for the highest derivative that the stencil size permits.

The 5×5 stencil corresponding to (10) is similarly obtained by approximating $f^{(24)}(0)$, giving

$$\begin{bmatrix} 1 & 16(-3+i) & 180 & 16(-3-i) & 1 \\ 16(-3-i) & -5440 & -24480 & -5440 & 16(-3+i) \\ 180 & -24480 & 119340 & -24480 & 180 \\ 16(-3+i) & -5440 & -24480 & -5440 & 16(-3-i) \\ 1 & 16(-3-i) & 180 & 16(-3+i) & 1 \end{bmatrix} f = 0 + O(h^{24}).$$

In this case, some of the entries are complex-valued. It depends on the context if this coupling between an analytic function's real and imaginary parts becomes a disadvantage, or can be used to advantage (as in Section 6 below). Real-valued stencils larger than (10) can readily be found. For example, including one more node in each direction of the two primary axes and considering $f^{(12)}(0)$ leads to

$$\begin{bmatrix} & & 1 & & \\ & -12 & -64 & -12 & \\ 1 & -64 & 300 & -64 & 1 \\ & -12 & -64 & -12 & \\ & & 1 & & \end{bmatrix} f = 0 + O(h^{12}).$$

5 Numerical analytic continuation

Numerical methods for analytic continuation are often very ill-conditioned. This section illustrates that the complex plane FD formula (11), applied in the form of (10) for verifying analyticity, can be applied successfully to this task.

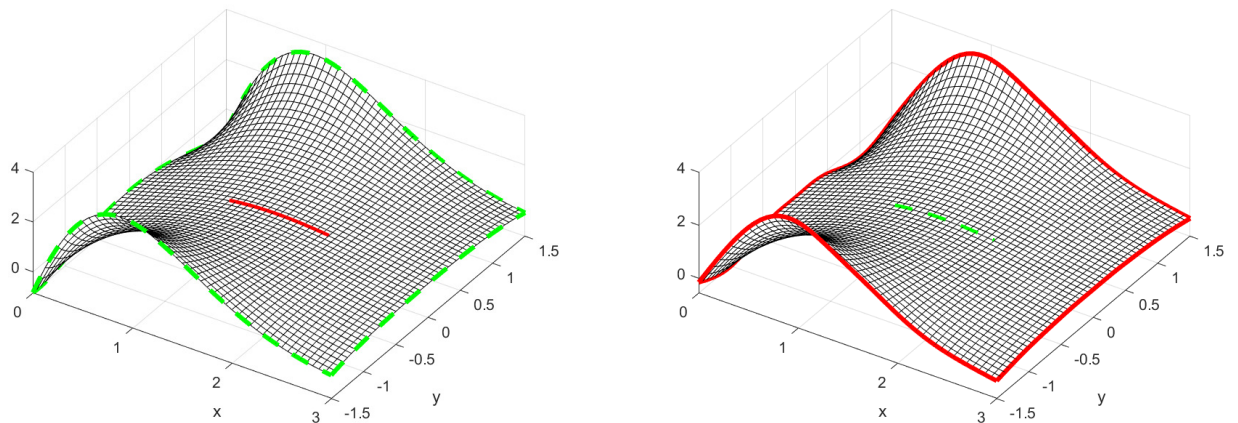
5.1 Boundary value problem for a harmonic function

Figure 4 (a) shows the real part of $1/\Gamma(z)$ over the complex plane region $[0, 3] \times [-1.5, 1.5]$. If one is given the function values around the edge of such a domain, it is straightforward to accurately approximate it throughout the domain interior, for example by applying (10) (ignoring its $O(h^8)$ error term) at each interior grid point. This gives rise to a well-conditioned sparse linear system. Assuming there is no singularity within the domain, the result will be accurate to $O(h^6)$. In particular, this provides function values along any interior line segment, such as the one shown in red in part (a) of the figure.

5.2 Analytic continuation

The reverse problem is to calculate the function across a full domain given values only for a small interior part of the domain. A key theorem tells that, if two analytic functions coincide on any curve segment, no matter how short (or on any infinite point set with a limit point), then the two functions are identical.⁸ The task of analytic continuation is to use such information (for example as provided by a Taylor series with finite radius of convergence) and then alter the functional representation to obtain a form that is defined in a larger region. Numerous analytic approaches

⁸See for ex. [13], Theorem 2.12.



(a) $\text{Re } 1/\Gamma(z)$ displayed over $[0, 3] \times [-1.5, 1.5]$.

(b) Numerical analytic continuation.

Figure 4: (a) Test function $\text{Re } 1/\Gamma(z)$, and (b) The result of numerical analytic continuation based only on the grid point data along the dashed green line (17 equidistant points extending over $1 \leq z \leq 2$).

for continuation are surveyed in [13]. Numerically, continuation is usually severely ill-conditioned, as analyzed in [23]. In its most immediate formulation, numerical continuation can be seen as solving Laplace's equation as an initial value problem.

5.3 FD-based numerical continuation

As a preliminary observation, we consider an over-determined linear system, where some equations $C\underline{x} = \underline{c}$ are to hold exactly, while others $A\underline{x} = \underline{b}$ are to be solved in the least squares sense (minimizing $\|A\underline{x} - \underline{b}\|_2$). The solution \underline{x} to this combination is obtained from the square linear system

$$\left[\begin{array}{c|c} A^T A & C^T \\ \hline C & 0 \end{array} \right] \begin{bmatrix} \underline{x} \\ \underline{\lambda} \end{bmatrix} = \begin{bmatrix} A^T \underline{b} \\ \underline{c} \end{bmatrix}, \quad (12)$$

where the $\underline{\lambda}$ -vector, containing Lagrange multipliers, can be ignored.

The continuation shown in Figure 4 (b) was obtained by

1. Enforce exactly: (i) Equation (10) (again ignoring its $O(h^8)$ error term) at all interior grid points, (ii) The input data (here the 17 function values at the equi-spaced grid points along $1 \leq z \leq 2$), and (iii) Agreement between the values along top and bottom boundaries (assuring symmetry around the real axis), and
2. Enforce in least square sense that the 3-point second derivative approximation (top line in Table 2) evaluates to zero when centered at all edge points of the computational domain (excepting the four corner points). Analytically, the second derivative should not be zero; enforcing this in least square sense is a (quite crude) way to suppress oscillations that otherwise would have been prominent around the boundaries.

Although the provided data (here 17 centerline points along the dotted green line segment in Figure 4 (b)) visually does not seem to provide much information, the approximate continuation nevertheless bears a lot of resemblance to the true function in Figure 4 (a). This example is only intended to illustrate the conceptual feasibility of quite direct FD approaches for continuation, leaving much room for further improvements.

Other numerical continuation methods are available especially when the data is available in other forms than (as in the current example) only at some low number of equi-spaced grid points. Continuation from data given at Chebyshev-type node sets is discussed in [22, 23]. In the case of data provided in the form of a truncated Taylor expansion, Padé expansions are often highly effective (and also capable of dealing quite well with functional singularities).

6 Approximation of harmonic conjugate functions

If the real part $u(x, y)$ of an analytic function $f(z)$ is given, the matching imaginary part $v(x, y)$ (known as the harmonic conjugate function) is determined by (2), apart from with respect to an arbitrary constant (and similarly if $v(x, y)$ is given). The simple complex plane FD relation

$$\frac{1}{h} \begin{bmatrix} -1 & 1 \end{bmatrix} v = \frac{1}{4h} \begin{bmatrix} -1 & -1 \\ 0 & 0 \\ 1 & 1 \end{bmatrix} u + O(h^2) \quad (13)$$

allows one to step v sideways from grid point to grid point (with an obvious counterpart stencil for stepping up/down). However, the second order accuracy of (13) is likely too low for practical use. The 'Method 1' can be used to provide generalizations in which the LHS stays the same (to allow easy node-by-node stepping) while the RHS (applied to known values) is extended in size. The following is one such example⁹

$$\frac{1}{h} \begin{bmatrix} -1 & 1 \end{bmatrix} v = \frac{1}{1064448 h} \begin{bmatrix} -1013 & -6253 & -6253 & -1013 \\ 23582 & 177346 & 177346 & 23582 \\ 149915 & -263861 & -263861 & 149915 \\ 0 & 0 & 0 & 0 \\ -149915 & 263861 & 263861 & -149915 \\ -23582 & -177346 & -177346 & -23582 \\ 1013 & 6253 & 6253 & 1013 \end{bmatrix} u + O(h^{12}) \quad (14)$$

$$\approx \frac{1}{h} \begin{bmatrix} -0.0010 & -0.0059 & -0.0059 & -0.0010 \\ 0.0222 & 0.1666 & 0.1666 & 0.0222 \\ 0.1408 & -0.2479 & -0.2479 & 0.1408 \\ 0 & 0 & 0 & 0 \\ -0.1408 & 0.2479 & 0.2479 & -0.1408 \\ -0.0222 & -0.1666 & -0.1666 & -0.0222 \\ 0.0010 & 0.0059 & 0.0059 & 0.0010 \end{bmatrix} u + O(h^{12}).$$

Although these weights numerically do not differ greatly from those of (13), the order of accuracy is much increased. Yet higher orders of accuracy are readily achieved by still larger stencils for u . Applying stencils such as (14) to step-by-step move sideways bears some resemblance to the

⁹Given the stencil size for u , this weight set is not unique, but it becomes unique if we impose the expected symmetries in the two directions.

quadrature procedure introduced in [4] (which however typically is less effective than end-corrected TR, cf., [9], Section 4.3).

7 Interpolation to a finer grid

A common task when given equi-spaced grid data is to interpolate to a twice as dense grid. It suffices for this to have a stencil for interpolating to the center location between two rows and columns, since turning such a stencil 45° will then allow remaining nodes on the finer grid to be filled in. The simplest such interpolation stencil can be written as

$$f(\odot) = \frac{1}{4} \begin{bmatrix} 1 & \odot & 1 \\ 1 & & 1 \end{bmatrix} f + O(h^4), \quad (15)$$

where \odot marks the center of a local square on the coarse grid. The next size stencil of this type is readily found (by either of Methods 1 or 2) to be

$$f(\odot) = \frac{1}{106496} \begin{bmatrix} -25 & 162 - 459i & 162 + 459i & -25 \\ 162 + 459i & 26325 & \odot & 26325 & 162 - 459i \\ 162 - 459i & 26325 & & 26325 & 162 + 459i \\ -25 & 162 + 459i & 162 - 459i & -25 & \end{bmatrix} f + O(h^{16}). \quad (16)$$

Between these two cases, the weights differ numerically no more than around $4 \cdot 10^{-3}$. For a general function $f(x, y)$ (not analytic), stencils of these sizes would at best be accurate to orders 2 and 4, respectively, scaling with the number of node points in each direction rather than, as here, with the total number of stencil nodes.

The error constant in the $O(h^{16})$ term in (16) will typically be small (unless interpolating near a singularity), making $h \approx 0.1$ sufficient for preserving the accuracy level of the grid data, up to the level of double precision (with a 6×6 stencil, $h \approx 0.35$ similarly suffices). While the weights will differ, the formal order of accuracy remains unchanged if the interpolation point is located arbitrarily relative to the node points that the interpolation is based on.

If one wishes to interpolate a harmonic function without having its harmonic conjugate available, it is convenient to have interpolation weights that are all real. This typically reduces the order of accuracy. For example, in the 4×4 stencil case¹⁰

$$f(\odot) = \frac{81}{1024} \begin{bmatrix} 13/81 & 1 & 1 & 13/81 \\ 1 & 1 & \odot & 1 \\ 1 & 1 & & 1 \\ 13/81 & 1 & 1 & 13/81 \end{bmatrix} f + O(h^{12}). \quad (17)$$

8 Weights for increasing stencil sizes

When using standard centered FD approximations along the real axis, and increasing the stencil width / order of accuracy for a fixed derivative, the weights converge to a limit known as the pseudospectral (PS) method [7, 21]. This is indicated in the bottom line of Tables 1 and 2, but valid more generally, cf., [7], Chapter 3. A serious problem in the 1-D case is that, in this limit,

¹⁰Method 1 can similarly be adapted to provide highly accurate FD formulas for derivatives of harmonic functions.

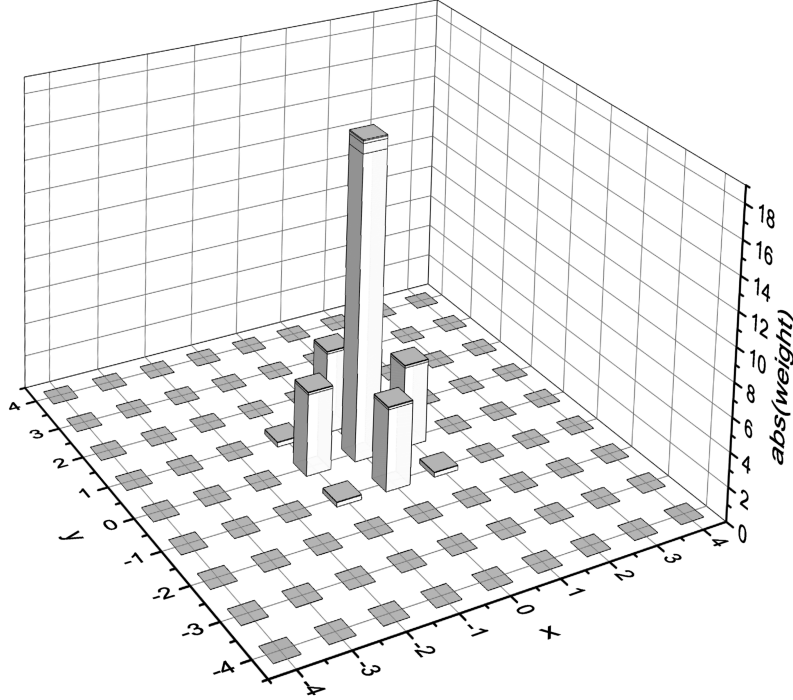


Figure 5: The magnitudes of the weights in the 9×9 complex stencil for the 4th derivative. The corresponding values for the 3×3 , 5×5 , and 7×7 stencils are indicated by thin lines near the tops of the bars. These stencils are accurate to orders $O(h^5)$, $O(h^{21})$, $O(h^{45})$, and $O(h^{77})$. The differences in weights are barely noticeable apart from near the top of the center column, illustrating the rapid convergence of the weights as the stencil sizes / orders of accuracy are increased. For the 9×9 stencil shown, the largest magnitude along the outer edge is around $4 \cdot 10^{-13}$ and the largest outside the central 3×3 area is around $3 \cdot 10^{-3}$.

the weights decay only very slowly, conflicting with the fact that a derivative is a completely ‘local’ property of a function. Figure 5 illustrates that, for increasing stencil sizes, weights in the complex FD case converge rapidly to a limit, and also that this limit is far more localized than in the PS case. We next give supporting analysis for these observations.

In the case of approximating the first derivative, with nodes at $z = z_k$, $k = 1, 2, \dots, N$, and with $N = 3^2, 5^2, 7^2$, Figure 6 compares two unit-spaced cases of approximations centered around $z = 0$: (i) nodes along the real axis (“FD real axis”) and (ii) nodes in a complex plane square (“FD complex plane”). In both cases, the center weight is zero, and is omitted. It shows in the latter case a far faster decay in the magnitude of the weights with node distance from the origin (i.e. these stencils rely much more on data near the point of interest)¹¹.

8.1 Approximations of the first derivative

For purposes of analysis, closed form expressions for FD weights w_k can be more convenient than the linear systems-based computational Methods 1 and 2 described in Section 2. By differentiating the Lagrange interpolation formula based on nodes located at $z = z_k$, $k = 1, 2, \dots, N$ (distinct, but

¹¹This is a key reason why these formulas can be highly effective also near singularities, as illustrated in Figures 2, 3.

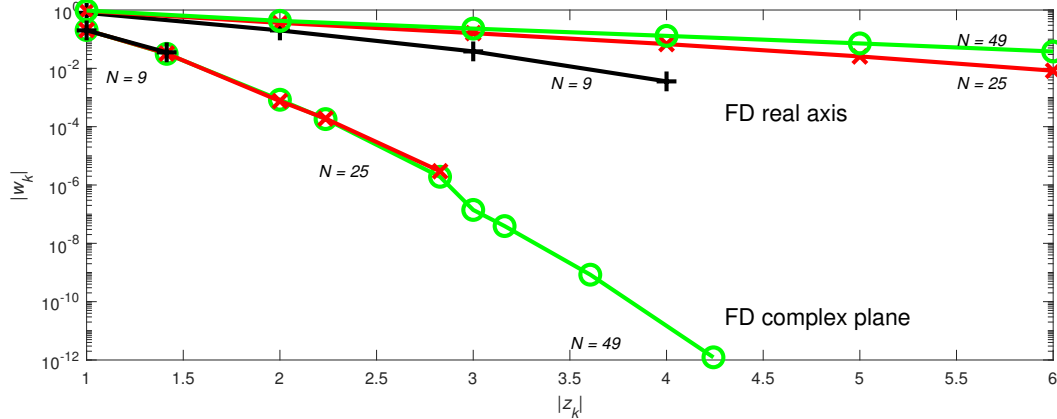


Figure 6: Magnitudes of weights w_k for centered approximations to the first derivative on unit-spaced grids, displayed on a log-linear scale against the distance of the respective node z_k from the origin. The “FD real axis” curves for $N = 25$ and $N = 49$ are truncated to the right. Increasing N (approaching a PS limit) severely damages locality for “FD real axis”, but not so for “FD complex plane”.

otherwise arbitrarily placed in the complex plane), one obtains for the first derivative at $z = 0$ the weights¹²

$$w_k = -\frac{1}{z_k} \left(\frac{d\phi}{dz} \Big|_{z=0} \right) / \left(\frac{d\phi}{dz} \Big|_{z=z_k} \right), \quad (18)$$

where

$$\phi(z) = \prod_{k=1}^N (z - z_k). \quad (19)$$

The decay in magnitude of the weights w_k (with the distance of z_k from the stencil center) depends therefore mostly on the rate of growth of $\left| \frac{d\phi}{dz} \right|$ with $|z|$.

8.1.1 Grid points along the real axis

As background before turning to the complex plane case, we note that (18), (19) reproduce the traditional PS method in the real-valued case. With unit-spaced nodes, (19) can be compared to the product $\frac{\sin \pi z}{\pi z} = \prod_{k=1}^{\infty} \left(1 - \frac{z^2}{k^2} \right)$. In the limit increasing N , the magnitude of the ratio $\left(\frac{d\phi}{dz} \Big|_{z=0} \right) / \left(\frac{d\phi}{dz} \Big|_{z=z_k} \right)$ in (18) approaches 1, and the weights will decay in magnitude according the remaining factor $\frac{1}{z_k}$ in (18), exactly matching the bottom line in Table 1. Growth of $\phi(z)$ with $|z|$ occurs in this limit only in directions away from the real axis, and does not assist in decreasing $|w_k|$.¹³

¹²Here, and later in (21), (22), one stencil node is assumed located at $z = 0$, with z_k a different node.

¹³Hermite-FD formulas approximate the p^{th} derivative, $p \geq 2$, using both function and first derivative values: $f^{(p)}(0) \approx \sum_{k=-n}^n b_k f(k) + \sum_{k=-n}^n c_k f'(k)$. Their infinite order PS limit is similar to that of regular FD-PS methods, as analyzed in [2].

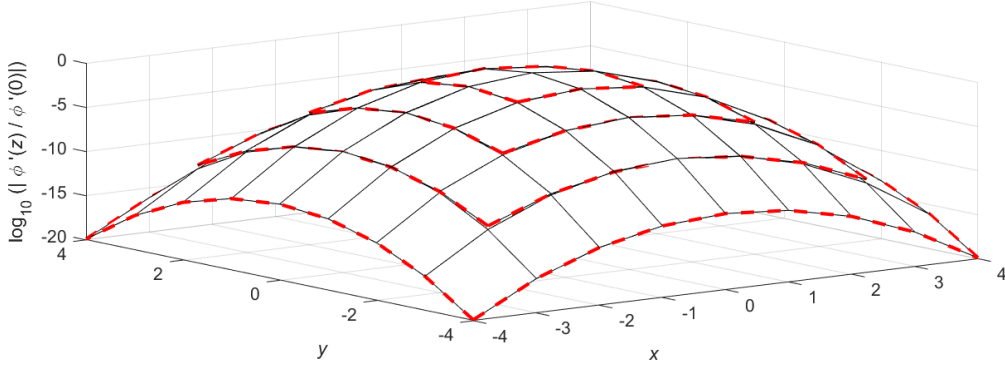


Figure 7: The magnitude of $\left(\frac{d\phi}{dz}\Big|_{z=0}\right) / \left(\frac{d\phi}{dz}\Big|_{z=z_k}\right)$ (log-linear display) at the node points of unit-spaced 3×3 , 5×5 , 7×7 , and 9×9 stencils. The outer edges of these stencils are highlighted by dashed red curves.

8.1.2 Grid points in the complex plane

In this case, $\phi(z)$ cannot, for $(2n + 1) \times (2n + 1)$ sized stencils with n increasing, converge to a bounded non-trivial limit function, since such a function would become doubly periodic and thus reduce to the constant zero. As a square stencil gets larger, rapid growth in magnitude of $|\phi'(z)|$ for increasing $|z|$ becomes inevitable. Figure 7 confirms this by displaying the magnitude of the ratio $\left(\frac{d\phi}{dz}\Big|_{z=0}\right) / \left(\frac{d\phi}{dz}\Big|_{z=z_k}\right)$ in the cases of 3×3 , 5×5 , 7×7 , and 9×9 unit spaced stencils, centered at the origin. The difference between the first two cases is graphically invisible, while a careful look at the corners of the 5×5 and 7×7 stencils, at locations $\pm 2 \pm 2i$, and $\pm 3 \pm 3i$, respectively, show a very small difference to the corresponding values of the next larger stencil.

In the limit of $n \rightarrow \infty$ and nodes $z_k = \mu + i\nu$, with μ, ν integers, it is shown in Appendix C that

$$\lim_{n \rightarrow \infty} \left| \left(\frac{d\phi}{dz}\Big|_{z=0}\right) / \left(\frac{d\phi}{dz}\Big|_{z=z_k}\right) \right| = e^{-\frac{\pi}{2}(\mu^2 + \nu^2)}. \quad (20)$$

The surfaces in Figure 7 (with the logarithmic vertical axis) thus converge to an axially symmetric paraboloid. Weights in unit-spaced complex plane FD formulas of increasing orders of accuracy thus decay roughly like the Gaussians $O(e^{-\frac{\pi}{2}|z_k|^2})$ with the distance of the stencil node z_k to the center node.

8.2 Generalizations to higher derivatives

Counterpart formulas to (18) are readily available also for higher derivatives. With the same assumptions as for (18), one obtains for the second derivative

$$w_k = - \left(\frac{2}{z_k^2} \left(\frac{d\phi}{dz}\Big|_{z=0}\right) + \frac{1}{z_k} \left(\frac{d^2\phi}{dz^2}\Big|_{z=0}\right) \right) / \left(\frac{d\phi}{dz}\Big|_{z=z_k}\right), \quad (21)$$

and for the third derivative

$$w_k = - \left(\frac{6}{z_k^3} \left(\frac{d\phi}{dz} \Big|_{z=0} \right) + \frac{3}{z_k^2} \left(\frac{d^2\phi}{dz^2} \Big|_{z=0} \right) + \frac{1}{z_k} \left(\frac{d^3\phi}{dz^3} \Big|_{z=0} \right) \right) / \left(\frac{d\phi}{dz} \Big|_{z=z_k} \right), \quad (22)$$

generalizing for the p^{th} derivative to

$$w_k = -p! \left(\sum_{\nu=1}^p \frac{1}{\nu! z_k^{p-\nu+1}} \left(\frac{d^\nu \phi}{dz^\nu} \Big|_{z=0} \right) \right) / \left(\frac{d\phi}{dz} \Big|_{z=z_k} \right). \quad (23)$$

In the complex FD case, the very rapid growth of $\left| \frac{d\phi}{dz} \right|$ away from the stencil center will lead to corresponding decreases in magnitude of the stencil weights (as $\left(\frac{d\phi}{dz} \Big|_{z=z_k} \right)$ enters in the denominators above). It is also apparent from (23) that the rates will depend very little on which order derivative is approximated. In the case of $(2n+1) \times (2n+1)$ unit-spaced stencils centered at $z=0$, it follows from symmetries that $\frac{d^p \phi}{dz^p} \Big|_{z=0} \neq 0$ only for $p = 1, 5, 9, 13, \dots$ causing terms in (21) - (23) to drop out. In the PS $n \rightarrow \infty$ limit, the ratios $\left(\frac{d^p \phi}{dz^p} \Big|_{z=0} \right) / \left(\frac{d\phi}{dz} \Big|_{z=0} \right)$ converge to constants.

9 Concluding discussion

FD formulas in the complex plane are generally considerably more accurate than traditional ones which use function values only along the real axis. Two reasons for this were outlined in the Introduction, both due to key aspects of analyticity. To these can be added the analysis in Section 8. Even as stencil sizes (and orders of accuracy) are increased, complex plane FD stencils continue to extract their main information from a very small neighborhood of the point of interest. This is in sharp contrast to traditional PS methods which, with their slow algebraic decay of weights, rely heavily on distant data even when approximating local operators, such as derivatives.

Holding a stencil size fixed and increasing the order p of the derivative $\frac{d^p}{dz^p}$ (as far as the stencil size permits) will typically make the weights (following the leading factor $1/h^p$) increase rapidly. The Euler-Maclaurin approximations described in Section 3 benefited from a compensating decrease in the magnitude of coefficients for the successive terms. If a very high order derivative is to be approximated, Cauchy integral-based algorithms (such as described in [5, 6]) may be preferable to FD approximations. Another option in that case might be to find FD weight sets where some orders of accuracy have been traded against reductions in the magnitude of the weights. This idea has been used successfully in contexts such as numerical quadrature (cf., [11, 16] in the cases of Gregory-type and Newton-Cotes-type formulas, respectively).

10 Appendix A: Code examples for the two weights algorithms

Let the task be to determine the weight set for the second derivative (i.e., $L = d^2/dz^2$) at the center of a 5×5 stencil. The next two sections illustrate how this can be done with the two methods described in Section 2. Comments indicate how to generalize to other node layouts and linear operators.

10.1 Method 1: MATLAB code

```
x = -2:2; zk = x-1i*x'; zk = zk(:).'; % Nodes z_k for 5x5 stencil (unit spaced)
A = zk.^((0:24)'); % Coefficient matrix for linear system to solve
v = zeros(25,1); v(3) = 2; % Form RHS; Set v(k+1) = k! for the k'th derivative
c2 = A\v; reshape(c2,5,5) % Solve for the weights and display in matrix form
```

For node spacing h , we replace $x = -2,2$; by $x = (-2,2)*h$. This code produces the same matrix as shown below for the Mathematica code, but as floating point numbers. Since the linear system is of Vandermonde-type, it is prone to numerical ill-conditioning. In the present test case, using standard double precision, about 4 digits get lost, leading to coefficient errors up to about 10^{-12} . Since the loss increases rapidly with stencil size, either exact rational or extended precision arithmetic is recommended (available in all common symbolic algebra packages). When using MATLAB, both are available through its symbolic toolbox; the latter also with the Advanpix toolbox¹⁴.

10.2 Method 2: Mathematica code

The following three Mathematica statements

```
zk = Flatten[Table[h (i - i j), {j, -2, 2}, {i, -2, 2}]]; (* Lay out nodes z_k *)
S =  $\xi^2 - \sum_{k=1}^{25} c[k] e^{-zk[[k]] \xi}$ ; (* With here  $L = \frac{d^2}{dz^2}$ ,  $L e^{e z} |_{z=0} = \xi^2$  *)
DM = Solve[LogicalExpand[Series[S, {\xi, 0, 24}] == 0]] (* Solve for the FD weights *)
```

computes the FD weights in closed form (with h as before denoting the node spacing). The further statement

```
MatrixForm[ArrayReshape[Table [c[k]/.DM[[1]],{k,1,25}],{5,5}]]
```

displays this set of weights in a standard matrix format:

$$\begin{pmatrix} -\frac{i}{477360 h^2} & -\frac{8}{149175} - \frac{8i}{49725} & \frac{1}{1326 h^2} & -\frac{8}{149175} + \frac{8i}{49725} & \frac{i}{477360 h^2} \\ \frac{8}{149175} + \frac{8i}{49725} & \frac{16i}{351 h^2} & -\frac{16}{39 h^2} & -\frac{16i}{351 h^2} & \frac{8}{149175} - \frac{8i}{49725} \\ -\frac{1}{1326 h^2} & \frac{16}{39 h^2} & \mathbf{0} & \frac{16}{39 h^2} & -\frac{1}{1326 h^2} \\ \frac{8}{149175} - \frac{8i}{49725} & -\frac{16i}{351 h^2} & -\frac{16}{39 h^2} & \frac{16i}{351 h^2} & \frac{8}{149175} + \frac{8i}{49725} \\ \frac{i}{477360 h^2} & -\frac{8}{149175} + \frac{8i}{49725} & \frac{1}{1326 h^2} & -\frac{8}{149175} - \frac{8i}{49725} & -\frac{i}{477360 h^2} \end{pmatrix}$$

¹⁴Multiprecision Computing Toolbox for MATLAB, <http://www.advanpix.com/>, Advanpix LLC, Yokohama, Japan.

11 Appendix B: Stencils of size 5×5 for the first four derivatives

$$\begin{aligned}
 f'(0) &= \frac{1}{h} \begin{bmatrix} \frac{1+i}{477360} & \frac{4(-1-i)}{29835} & \frac{i}{1326} & \frac{4(1-i)}{29835} & \frac{-1+i}{477360} \\ \frac{4(-1-i)}{29835} & \frac{8(-1-i)}{351} & \frac{-8i}{39} & \frac{8(1-i)}{351} & \frac{4(1-i)}{29835} \\ \frac{1}{1326} & \frac{-8}{39} & 0 & \frac{8}{39} & \frac{-1}{1326} \\ \frac{4(-1+i)}{29835} & \frac{8(-1+i)}{351} & \frac{8i}{39} & \frac{8(1+i)}{351} & \frac{4(1+i)}{29835} \\ \frac{1-i}{477360} & \frac{4(-1+i)}{29835} & \frac{-i}{1326} & \frac{4(1+i)}{29835} & \frac{-1-i}{477360} \end{bmatrix} f + O(h^{24}), \\
 f''(0) &= \frac{1}{h^2} \begin{bmatrix} \frac{-i}{477360} & \frac{8(-1+3i)}{149175} & \frac{1}{1326} & \frac{8(-1-3i)}{149175} & \frac{i}{477360} \\ \frac{8(1+3i)}{149175} & \frac{16i}{351} & \frac{-16}{39} & \frac{-16i}{351} & \frac{8(1-3i)}{149175} \\ \frac{-1}{1326} & \frac{16}{39} & 0 & \frac{16}{39} & \frac{-1}{1326} \\ \frac{8(1-3i)}{149175} & \frac{-16i}{351} & \frac{-16}{39} & \frac{16i}{351} & \frac{8(1+3i)}{149175} \\ \frac{i}{477360} & \frac{8(-1-3i)}{149175} & \frac{1}{1326} & \frac{8(-1+3i)}{149175} & \frac{-i}{477360} \end{bmatrix} f + O(h^{23}), \\
 f^{(3)}(0) &= \frac{1}{h^3} \begin{bmatrix} \frac{-1+i}{636480} & \frac{8(7-i)}{248625} & \frac{-i}{884} & \frac{8(-7-i)}{248625} & \frac{1+i}{636480} \\ \frac{8(1-7i)}{248625} & \frac{8(1-i)}{117} & \frac{16i}{13} & \frac{8(-1-i)}{117} & \frac{8(-1-7i)}{248625} \\ \frac{1}{884} & \frac{-16}{13} & 0 & \frac{16}{13} & \frac{-1}{884} \\ \frac{8(1+7i)}{248625} & \frac{8(1+i)}{117} & \frac{-16i}{13} & \frac{8(-1+i)}{117} & \frac{8(-1+7i)}{248625} \\ \frac{-1-i}{636480} & \frac{8(7+i)}{248625} & \frac{i}{884} & \frac{8(-7+i)}{248625} & \frac{1-i}{636480} \end{bmatrix} f + O(h^{22}), \\
 f^{(4)}(0) &= \frac{1}{h^4} \begin{bmatrix} \frac{1}{318240} & \frac{32(-9-13i)}{1243125} & \frac{-1}{442} & \frac{32(-9+13i)}{1243125} & \frac{1}{318240} \\ \frac{32(-9+13i)}{1243125} & \frac{-32}{117} & \frac{64}{13} & \frac{-32}{117} & \frac{32(-9-13i)}{1243125} \\ \frac{-1}{442} & \frac{64}{13} & \frac{-92937}{5000} & \frac{64}{13} & \frac{-1}{442} \\ \frac{32(-9-13i)}{1243125} & \frac{-32}{117} & \frac{64}{13} & \frac{-32}{117} & \frac{32(-9+13i)}{1243125} \\ \frac{1}{318240} & \frac{32(-9+13i)}{1243125} & \frac{-1}{442} & \frac{32(-9-13i)}{1243125} & \frac{1}{318240} \end{bmatrix} f + O(h^{21}).
 \end{aligned}$$

For this stencil size, one can approximate up through $f^{(24)}(0)$ which then becomes first order accurate.

12 Appendix C:

Following up on Section 8, we consider again

$$\begin{aligned}
 \phi(z) &= \prod_{\eta=1}^N (z - z_\eta) = \prod_{\substack{\mu = -n, \dots, +n \\ \nu = -n, \dots, +n}} (z - (\mu + i\nu)),
 \end{aligned}$$

and note that

$$\phi'(z_k) = \prod_{\substack{\eta=1 \\ \eta \neq k}}^N (z_k - z_\eta). \quad (24)$$

We next refer to Figure 8, with a schematic illustration in the $n = 4$ case (with a total of $N = (2n + 1)^2 = 81$ nodes), and $\mu = 2, \nu = 1$, i.e., $z_k = 2 + i$ (marked by a triangle, in contrast to $z = 0$ marked by a square). The value for $\phi'(0)$, according to (24), is obtained by a product over all nodes inside the large solid square (omitting its center node). If the corresponding product for $\phi'(z_k)$ had used the nodes inside the dashed square (again omitting the center node), it would have evaluated to the same result. However, it does not, but a calculation for $\log |\phi'(0)|$ becomes a calculation for $\log |\phi'(z_k)|$ if we to it add the sums

$$S_1 = \sum_{z_\eta \text{ in rectangle 1}} \log |z_\eta|, \quad S_2 = \sum_{z_\eta \text{ in rectangle 2}} \log |z_\eta|$$

and subtract

$$S_3 = \sum_{z_\eta \text{ in rectangle 3}} \log |z_\eta|, \quad S_4 = \sum_{z_\eta \text{ in rectangle 4}} \log |z_\eta|.$$

Each of these four sums is readily estimated to leading order. Along the center line of each of the four narrow rectangles (marked 1, 2, 3, 4 in the figure) we can approximate the sum by suitable use of the integral relation

$$\int_a^b \log(x^2 + y^2) dx = 2y \left(\arctan \frac{b}{y} - \arctan \frac{a}{y} \right) + b (\log(b^2 + y^2) - 2) - a (\log(a^2 + y^2) - 2)$$

together with multiplying each integral by the width (orthogonal to the center line) of the respective rectangle. After straightforward algebra, this gives

$$S_1 + S_2 - S_3 - S_4 = \frac{\pi}{2}(\mu^2 + \nu^2) - \frac{1}{2n}(\mu^2 + \nu^2) + O\left(\frac{1}{n^2}\right), \quad (25)$$

from with (20) then follows.

Declarations: No funding was received for the present work. The author has no conflict of interest.

References

- [1] J. Abate and H. Dubner, *A new method for generating power series expansion of functions*, SIAM J. Numer. Anal. **5** (1968), 102–112.
- [2] D. Abrahamsen and B. Fornberg, *On the infinite order limit of Hermite-based finite difference schemes*, SIAM J. Numer. Anal. **59** (2021), no. 4, 1857–1874.
- [3] L.V. Ahlfors, *Complex Analysis*, McGraw-Hill, New York, 1966.
- [4] G. Birkhoff and D. Young, *Numerical quadrature of analytic and harmonic functions*, J. Math. Physics **29** (1950), 217–221.
- [5] F. Bornemann, *Accuracy and stability of computing high-order derivatives of analytic functions by Cauchy integrals*, Found. Comput. Math. **11** (2011), 1–63, doi: 10.1007/s10208-010-9075-z.

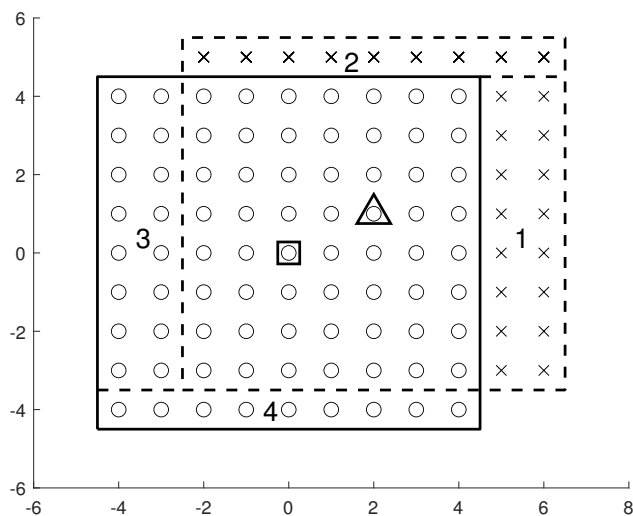


Figure 8: Illustration of the node sets used in the estimate of the sums S_1, \dots, S_4 , as described in Appendix C.

- [6] B. Fornberg, *Numerical differentiation of analytic functions*, ACM Trans. Math. Software **7** (1981), no. 4, 512–526.
- [7] ———, *A Practical Guide to Pseudospectral Methods*, Cambridge University Press, 1996.
- [8] ———, *Euler-Maclaurin expansions without analytic derivatives*, Proc. Royal Soc. London, Series A **476** (2020), no. 20200441, doi: 10.1098/rspa.2020.0441.
- [9] ———, *Contour integrals of analytic functions given on a grid in the complex plane*, IMA J. Numer. Anal. **41** (2021), 814–825, doi:10.1093/imanum/draa024.
- [10] ———, *Generalizing the trapezoidal rule in the complex plane*, Numerical Algorithms **87** (2021), 187–202.
- [11] ———, *Improving the accuracy of the trapezoidal rule*, SIAM Review **63** (2021), no. 1, 167–180.
- [12] B. Fornberg and N. Flyer, *A Primer on Radial Basis Functions with Applications to the Geosciences*, CBMS-NSF, vol. 87, SIAM, Philadelphia, 2015.
- [13] B. Fornberg and C. Piret, *Complex Variables and Analytic Functions: An Illustrated Introduction*, SIAM, Philadelphia, 2020.
- [14] B. Fornberg and J.A.C. Weideman, *A numerical methodology for the Painlevé equations*, J. Comput. Phys. **230** (2011), 5957–5973.
- [15] J.H. Hinojosa and K.L. Mickus, *Hilbert transform of gravity gradient profiles: Special cases of the general gravity-gradient tensor in the Fourier transform domain*, Geophysics **67** (2002), no. 3, 766–769.
- [16] D. Huybrechs, *Stable high-order quadrature rules with equidistant points*, Comput. Appl. Math. **231** (2009), 933–947.

- [17] R.J. LeVeque, *Finite Difference Methods for Ordinary and Partial Differential Equations*, SIAM, Philadelphia, 2007.
- [18] J.N. Lyness and C.B. Moler, *Numerical differentiation of analytic functions*, SIAM J. Numer. Anal. **4** (1967), 202–210.
- [19] J.N. Lyness and G. Sande, *Algorithm 413-ENTCAF and ENTCRE: Evaluation of normalized Taylor coefficients of an analytic function*, Comm. ACM **14** (1971), no. 10, 669–675.
- [20] L.F. Richardson, *On the approximate arithmetical solution by finite differences of physical problems involving differential equations, with an application to the stresses in a masonry dam*, Proc. Royal Soc. A. **83** (1910), 307–357, doi:<https://doi.org/10.1098/rspa.1910.0020>.
- [21] L.N. Trefethen, *Spectral Methods in MATLAB*, SIAM, Philadelphia, 2000.
- [22] L.N. Trefethen, *Approximation Theory and Approximation Practice*, SIAM, Philadelphia, 2013, extended edition 2019.
- [23] L.N. Trefethen, *Quantifying the ill-conditioning of analytic continuation*, BIT Numer. Math. **60** (2020), 901–915.